Physics Letters A 572 (2026) 131315

Contents lists available at ScienceDirect

Physics Letters A

journal homepage: www.elsevier.com/locate/pla

Letter

Magnetic topological phases in the bulk van der Waals crystals $EuBi_4Te_7$ and $EuSb_4Te_7$

Jia-Yi Lin, Xiao-Bao Yang, Yu-Jun Zhao *

Department of Physics, South China University of Technology, Guangzhou, 510640, PR China

ARTICLE INFO

Editor: Dr. MingZhong Wu

Keywords:
Magnetic topological phase
Topological surface state
Magnetic symmetry
First-principles calculation

ABSTRACT

In the past several years, magnetic topological materials have attracted interests since the exotic physical phenomena unveiled on these platforms. Using first-principles calculations, we predict that two new-type magnetic van der Waals crystals, $EuBi_4Te_7$ and $EuSb_4Te_7$, are topologically nontrivial with multiple topological phases in various magnetic configurations. In their magnetic ground states, coexisting antiferromagnetic topological insulator phase and axion insulator phase are identified. Therefore, massless Dirac fermion dispersions appear on the surfaces parallel to the out-of-plane orientation. When magnetized to ferromagnetic states, axion insulator phases protected by parity symmetry survive. Meanwhile, if the spins align along the *x* direction, they are mirror topological crystalline insulators with massless Dirac cones on their (001) and (010) surfaces. The magnetic easy axes of $EuBi_4Te_7$ and $EuSb_4Te_7$ are along the in-plane and out-of-plane orientations, respectively. These findings open more opportunities for the research and application of magnetic topological physics and topological quantum phase transitions.

Introduction

In the past two decades, topological quantum physics have become one of the most fantastic subject in the modern condensed matter physics [1]. Since the earliest concept model was conceived, dozens of topological quantum states and topological quantum phases in condensed matter have been proposed theoretically and realized experimentally [2–4]. On the one hand, a series of novel dissipationless quantum transport phenomena, such as the quantum integer Hall effect, quantum spin Hall effect, quantum anomalous Hall effect and fractional quantum Hall effect, have been discovered in the topological material platforms [5,6]. These quantum Hall transport phenomena, are expected to be promising for the quantum superconductor, quantum computation and next generation spintronic device application [7]. On the other hand, there are different kinds of quasi-particle dispersion relations in the topological condensed matter, such as the Dirac fermion, Weyl fermion and Majorana fermion, which enlighten the research of the basic theoretical physics since these quasi-particles subject to the same form of Hamiltonians and motion equations with the basic particles [8,9].

In the early times, the searches for materials with nontrivial band topology are most concentrated on the nonmagnetic systems. A great number of representative nonmagnetic topological materials are unveiled, such as the Bi_2Se_3 topological insulator (TI) family, the Cd_3As_2 and Na_3Bi Dirac semimetals, the TaAs Weyl semimetal family, the SnTe topological crystalline insulator (TCI) family, the higher-order topological insulator in Bismuth and the higher-order topological semimetals [10–20]. Several nonmagnetic topological material databases have been established in 2019 [21–23]. Especially, all topological bands of all nonmagnetic materials in the Inorganic Crystal Structure Database (ICSD) have been screened by Bernevig *et al.* in 2022 [24]. It appears that the high-throughput screen for nonmagnetic topological electronic materials is well-established. Additionally, the topological phonon material database also have been established by Xu *et al.* recently [25].

Unlike the rapid development of the research for the nonmagnetic counterparts, however, the study of the magnetic topological quantum phases is hindered by the insufficiency of real material realizations. This is partially because the theoretical calculations for the magnetic materials are more or less ambiguous for the strongly correlated electrons of the magnetic atoms, which are much more complex than the nonmagnetic systems. Furthermore, different magnetic configurations would give rise to various magnetic symmetries, which makes the determination of the topological phases of magnetic systems more difficult and clearly more complicated than the symmetries found in nonmagnetic systems. Nevertheless, since the strongly coupling between the magnetic topological phases and the magnetic configurations, there are novel properties in the magnetic topological materials that cannot be

* Corresponding author.
E-mail addresses: 752917623@qq.com (J.-Y. Lin), scxbyang@scut.edu.cn (X.-B. Yang), zhaoyj@scut.edu.cn (Y.-J. Zhao).

https://doi.org/10.1016/j.physleta.2025.131315
Received 3 September 2025; Received in revised form 16 November 2025; Accepted 28 December 2025
Available online 1 January 2026

achieved on the nonmagnetic platforms. For instance, multiple magnetic topological phases and magnetically controllable quantum phase transitions can be expected on these material platforms. Different from the intrinsic magnetic moments in the crystals, the applied external magnetic field will break the translation symmetries and the periodic boundary conditions which are along the directions that are vertical to the magnetic field, giving rise to the Landau levels [26,27]. Therefore, searching more magnetic topological materials is desirable both theoretically as well as experimentally.

Although the earlist concept model of the antiferromagnetic (AFM) TI have been proposed in 2010 [28], the first AFM TI is not discovered until 2019, when the nontrivial band topology is revealed in the $MnBi_2Te_4$ bulk van der Waals (vdW) crystal [29]. In the interlayer antiferromagnetic (A-AFM) ground state, $MnBi_2Te_4$ is an AFM TI as well as an axion insulator (AXI) [30]. When magnetized to the ferromagnetic (FM) configurations, Weyl semimetal phases are obtained. In the $MnBi_2Te_4$ thin films with a few number of layers, the Chern insulator phases can be realized [31,32]. Similar physical phenomena, also have been predicted in $MnSb_2Te_4$ [33]. The TI phase, is observed in the $MnBi_2Se_4$ material likewise [34]. Recently, the second order topological phase is unveiled in $MnBi_2Te_4$ films [35].

As for the close relatives of the $MnBi_2Te_4$ and $MnSb_2Te_4$, the vdW material families $MnBi_2Te_4{\cdot}(Bi_2Te_3)_n$ and $MnSb_2Te_4{\cdot}(Sb_2Te_3)_n$ have been diagnosed as magnetic topological material candidates and realized in experiments in the past several years [36–40]. The magnetic ground states of these compounds can be easily tuned since the interlayer magnetic couplings are weak [41,42]. In $Mn_2Bi_2Te_5$ and $Mn_2Sb_2Te_5$, AFM TI or AXI phases and ferromagnetic AXI or Weyl semimetal phases are also predicted theoretically [43–46]. The TCI phases, are predicted in the FM*x* configurations in these material families [47–49]. High temperature quantum anomalous Hall effect is observed in experiments in $MnBi_4Te_7$ as well [50].

In this work, we predict that $EuBi_4Te_7$ and $EuSb_4Te_7$ are magnetic topological material candidates using first-principles calculations. In the A-AFM magnetic ground state, AFM TI phase and AXI phase coexist regardless of their different magnetic easy axes. As a result, Dirac fermion dispersions are discovered on their surfaces. In the ferromagnetic configurations, AXI phases are obtained as the parity symmetry survived. When the spins align along the *x* direction parallelly or anti-parallelly, the TCI phases emerge and the massless Dirac cones appear on their (010) and (001) surfaces. The phonon dispersions without imaginary frequency imply the dynamical stabilities of these compounds.

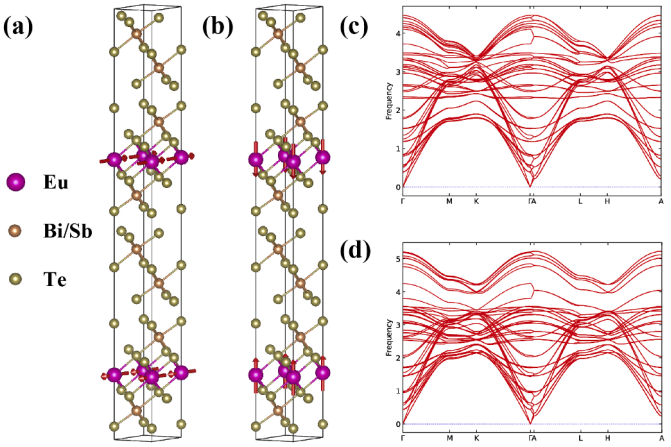

Fig. 1. The crystal structures and phonon dispersions with the A-AFM magnetic ground states of $EuBi_4Te_7$ and $EuSb_4Te_7$. **(a)** The crystal structure of $EuBi_4Te_7$, **(b)** the crystal structure of $EuSb_4Te_7$, **(c)** the phonon dispersion of $EuBi_4Te_7$, **(d)** the phonon dispersion of $EuSb_4Te_7$.

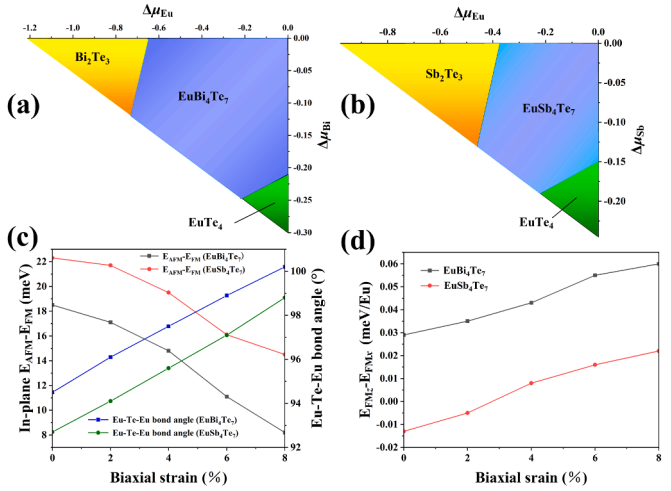

Fig. 2. The chemical potential ranges, in-plane magnetic exchange energies and magnetic anisotropy energies of $EuBi_4Te_7$ and $EuSb_4Te_7$. **(a)** The chemical potential range of $EuBi_4Te_7$, **(b)** the chemical potential range of $EuSb_4Te_7$, **(c)** the in-plane magnetic exchange energies, **(d)** the magnetic anisotropy energies.

Methods

All the calculations were performed based on density functional theory (DFT) with the Vienna *ab initio* simulation package (VASP) [51–53]. The generalized gradient approximation (GGA) level Perdew-Burke-Ernzerhof (PBE) functional for the exchange-correlation energy is adopted [54]. The projector-augmented wave (PAW) pseudopotentials were employed [55,56]. We set an energy cutoff of 375 eV for the plane wave basis set to expand the Kohn-Sham wavefunctions [57]. The criterion for the energy convergence of the electronic self-consistent field (SCF) calculations was no more than 1×10^{-8} eV/cell and the coordinations of all atoms were fully relaxed until the Hellmann-Feynman forces were smaller than 1×10^{-4} eV/Å. The spin-orbit coupling (SOC) effect is included throughout our calculations. In order to appropriately included the strongly correlated effect of the Eu 4*f* electrons, we employed the DFT + U method with an effective U value of 7 eV [58,59]. We have tested the U values of 6 eV, 7 eV and 8 eV with the PBE functional and the U value of 7 eV with a more accurate metaGGA R^2SCAN functional [60,61], which yield the same magnetic ground states and topological symmetry indicators (SIs). To appropriately include the vdW interactions, the DFT-D4 dispersion correction method is employed [62,63]. An 18×18×4 Γ-centered *k*-mesh is adoped for the calculations. The formation enthalpy and chemical potential ranges are calculated via the R^2SCAN functional. We calculated the band representations and topological SIs via the irvsp, TopMat and Mvasp2trace codes [64,65]. The Wannier Hamiltonians were constructed by the Wannier90 package [66–68]. To construct the Wannier Hamiltonians, the Eu 4*f*, Bi 6*p*, Sb 5*p* and Te 5*p* orbitals are included in the projections. To maintain the symmetries of the Hamiltonians, zero step of the wannierization procedure was set. The surface state spectra were simulated by the WannierTools package using the iterative Green function method [69,70].

Results and discussions

The crystal structures with the A-AFM magnetic ground states of $EuBi_4Te_7$ and $EuSb_4Te_7$ are shown in Fig. 1(a)(b). These compounds consist of an Eu(Bi, Sb)$_2$Te$_4$ septuple layer (SL) and a (Bi, Sb)$_2$Te$_3$ quintuple layer (QL) in their primitive cell, stacked along the *c* axis via weak vdW interaction. They belong to the $P\bar{3}m1$ (No. 164) space group. In our calculations, the energies of the A-AFM ground states are 2.389 meV/Eu and 0.895 meV/Eu lower than the FM energies in $EuBi_4Te_7$ and $EuSb_4Te_7$, respectively. However, their magnetic easy axes we predicted are different. The energy of FM*x* state is 0.029 meV/Eu lower than the

FMz energy in $EuBi_4Te_7$. In $EuSb_4Te_7$, the energy of FMz state is 0.013 meV/Eu lower than that of FMx state. The in-plane magnetic ordering is also determined via the $2\times1\times1$ supercell. In our calculations, the in-plane FM configuration is more stable than the in-plane AFM configuration in both $EuBi_4Te_7$ and $EuSb_4Te_7$. The in-plane E_{AFM}-E_{FM} is 18.5 meV/Eu for $EuBi_4Te_7$ and 22.3 meV/Eu for $EuSb_4Te_7$. Such relatively large energy difference indicates that the in-plane FM coupling is robust. To explore the magnetic exchange mechanism, we have calculated the in-plane E_{AFM}-E_{FM} and the Eu-Te-Eu bond angles under biaxial strain conditions. We find that the Eu-Te-Eu bond angle is enlarged from about 94.5° to 100.2° for $EuBi_4Te_7$ and 92.7° to 98.8° for $EuSb_4Te_7$ as biaxial strained from 0 to 8%. Meanwhile, the in-plane ferromagnetism is degraded in this process, as shown in the Fig. 2(c). This is a typical feature of the super exchange interaction according to the Goodenough-Kanamori rule [71]. Therefore, we conclude that the in-plane magnetic exchange is the Eu-Te-Eu super exchange. As for the interlayer magnetic interactions, the distance between two Eu layer is relatively far and separated by the vdW gap. It seems that the wavefunctions of the Eu atoms of different layer are difficult to exchange with each other. We find that the calculated band gap in interlayer AFM configuration is 89.8 meV and 87.3 meV for $EuBi_4Te_7$ and $EuSb_4Te_7$, respectively. In the interlayer FM configuration, these values are 81.87 meV and 77.01 meV. We expect that the larger band gap in the interlayer AFM configuration give rise to a lower total electron energy and the interlayer AFM magnetic ground states. In the $EuTe_6$ octahedron crystal field, the spherical symmetric of the Eu f wavefunctions are broken down, which give rise to the magnetic anisotropy. As shown in Fig. 2(d), under biaxial strain conditions, the in-plane magnetic easy axis is more favored in both $EuBi_4Te_7$ and $EuSb_4Te_7$.

As shown in Fig. 1(c)(d), there is no soft mode which is manifested as negative frequencies in the phonon dispersion. In the literatures, soft modes initiate lattice instability that potentially induces a structural phase transition and thus synthesizing the compound with soft mode phonon dispersion under normal conditions may be challenging [72]. In the study of materials, the absence of the soft mode in the phonon dispersion curve indicates dynamic stability [73]. Therefore, the $EuBi_4Te_7$ and $EuSb_4Te_7$ are dynamically stable based on our calculated phonon dispersions.

Furthermore, the formation enthalpy (ΔH) of the $EuBi_4Te_7$ and $EuSb_4Te_7$ compound is now calculated to confirm their thermodynamic stability, which is dependent on the energy of all of the constituent elements:

$$\Delta H(EuM_4Te_7) = E_{tot}^{EuM_4Te_7} - (E^{Eu} + 4E^{M} + 7E^{Te}), \quad (1)$$

where M = Bi, Sb. According to our calculation results, the formation enthalpy is -1.21 eV and -0.98 eV for $EuBi_4Te_7$ and $EuSb_4Te_7$, respectively. The negative values of the formation enthalpy indicate their possible thermodynamic stability.

Then we calculate the stable chemical potential ranges of $EuBi_4Te_7$ and $EuSb_4Te_7$ to avoid possible competing phases. We define:

$$\mu_\alpha = \mu_\alpha^{solid} + \Delta\mu_\alpha. \quad (2)$$

where μ_α is the element chemical potential, and μ_α^{solid} equals to $-E_{coh}(\alpha)$. $-E_{coh}(\alpha)$ stands for the cohesive energy of the corresponding element crystal. The atomic chemical potential should be smaller than that of their corresponding elemental solid to avoid precipitation of solid elemental crystal. That is:

$$\Delta\mu_{Eu} \le 0, \Delta\mu_{Bi} \le 0, \Delta\mu_{Te} \le 0. \quad (3)$$

The sum of chemical potentials for all atoms equals to the formation enthalpy of the compound to maintain a stable compound. That is:

$$\Delta\mu_{Eu} + 4\Delta\mu_{Bi} + 7\Delta\mu_{Te} = \Delta H(EuBi_4Te_7). \quad (4)$$

The chemical potentials are further restricted with their other possible competing phases:

$$\Delta\mu_{Eu} + 4\Delta\mu_{Te} \le \Delta H(EuTe_4), \quad (5)$$

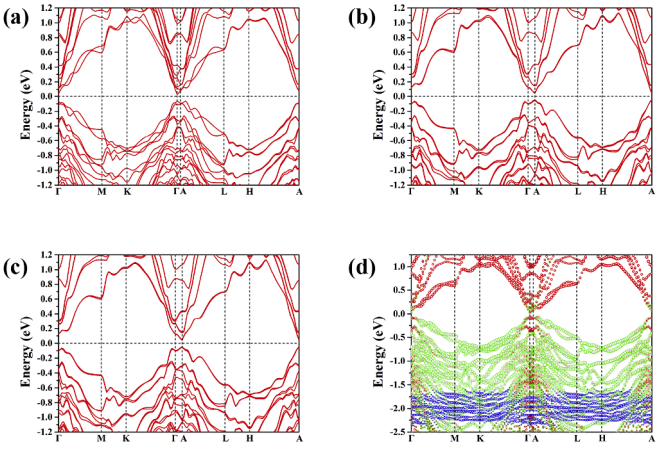

Fig. 3. The band structures of $EuBi_4Te_7$. The bulk band structure of $EuBi_4Te_7$ in **(a)** A-AFMx configuration, **(b)** FMx configuration, **(c)** FMz configuration, **(d)** the projected band structure in A-AFMx configuration, in which the red bubbles represent the Bi p orbital projection, the green bubbles represent the Te p orbital projection and the blue bubbles represent the Eu f orbital projection.

and

$$2\Delta\mu_{Bi} + 3\Delta\mu_{Te} \le \Delta H(Bi_2Te_3). \quad (6)$$

Following the same procedure, the chemical potential range of $EuSb_4Te_7$ can be obtained as the $EuBi_4Te_7$. The obtained stable chemical potential ranges of $EuBi_4Te_7$ and $EuSb_4Te_7$ are shown as Fig. 2(a)(b). Therefore, we conclude that $EuBi_4Te_7$ and $EuSb_4Te_7$ are stable according to our calculation results.

The calculated bulk band structures in the A-AFMx, FMx and FMz configurations of $EuBi_4Te_7$ are shown in Fig. 3(a)–(c), respectively. In the A-AFMx magnetic ground state, a band gap of 89.8 meV is opened near the Γ point. As shown in Fig. 3(d), a band inversion between the Bi p and Te p orbitals appears near the Γ point, which is a hallmark of the topological materials. The occupied Eu 4f flat bands are located at the energy of about 1.7 eV to 2.3 eV below the Fermi energy. Although the Eu 4f bands lies well below the Fermi energy, their energy range still overlaps that of the Te 5p bands. Therefore, there are still interactions between the Eu 4f bands and other bands, which can influence the surface states. Furthermore, the inverted bulk band gap and the magnetic symmetry of the magnetic configurations determine the topological surface or hinge states on certain surfaces/hinges. The magnetic space group of the A-AFMx $EuBi_4Te_7$ is C_c2/m (No. 12.63), containing the parity symmetry $\hat{P}$ and the time-reversal combined with a fractional translation symmetry $\hat{S} = \hat{T}\tau_{\frac{1}{2}}$. Therefore, all the bands are in double degeneracy as Kramer pairs with spin up and spin down states. In the FM configurations, such Kramer degeneracy is lifted by the magnetization as the $\hat{S}$ symmetry is broken.

Based on the $\hat{S}$ and the $\hat{P}$ symmetries, the band topology can be diagnosed by the $\mathbb{Z}_2$ topological invariant written as follow:

$$(-1)^\lambda = \prod_{k_{inv}, n\in occ/2} \xi_n(k_{inv}), \quad (7)$$

where k_{inv} is the time-reversal invariant k points in the first Brillouin zone, n runs over all the occupied Kramer pairs of the energy bands and λ is the $\mathbb{Z}_2$ topological invariant [74]. Using Eq. (7), a nontrivial $\mathbb{Z}_2 = 1$ is obtained, indicating that $EuBi_4Te_7$ is an AFM TI in its magnetic ground state. Since the parity symmetry $\hat{P}$ exist, the band topology can also be identified by the $\mathbb{Z}_4$ topological invariant as follows:

$$\mathbb{Z}_4 = \sum_{\alpha=1}^{8}\sum_{n=1}^{n_{occ}} \frac{1+\xi_n(\Lambda_\alpha)}{2} \mod 4, \quad (8)$$

where Λ_α represents the eight inversion invariant k points in the first Brillouin zone, n runs over all the occupied energy bands, and $\xi_n(\Lambda_\alpha)$ is

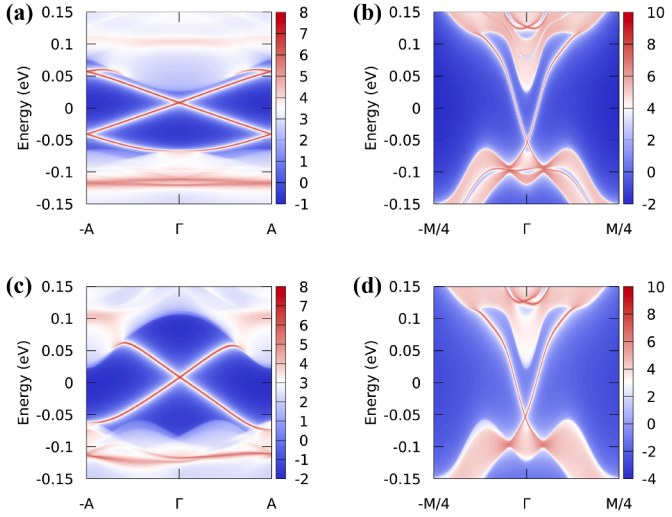

Fig. 4. The simulated surface spectra of $EuBi_4Te_7$. The surface LDOS of $EuBi_4Te_7$ in the A-AFM*x* configuration on **(a)** the (010) surface, **(b)** the (001) surface, in the FM*x* configuration on **(c)** the (010) surface, **(d)** the (001) surface.

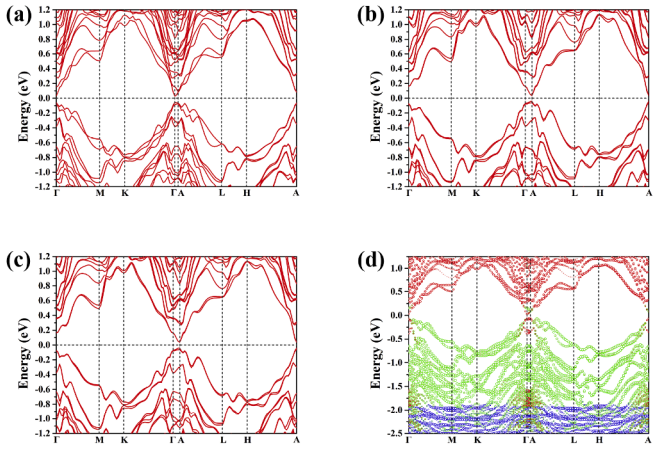

Fig. 5. The band structures of $EuSb_4Te_7$. The bulk band structure of $EuSb_4Te_7$ in **(a)** A-AFM*z* configuration, **(b)** FM*x* configuration, **(c)** FM*z* configuration, **(d)** the projected band structure in A-AFM*z* configuration, in which the red bubbles represent the Sb *p* orbital projection, the green bubbles represent the Te *p* orbital projection and the blue bubbles represent the Eu *f* orbital projection.

the parity eigenvalue of the *n*th energy band at Λ_α [75,76]. It is demonstrated that $\mathbb{Z}_4 = 1$ or 3 indicates a topological semimetal phase and $\mathbb{Z}_4 = 2$ indicates an AXI phase, while $\mathbb{Z}_4 = 0$ suggests a topological trivial phase. Via Eq. (8), we obtained $\mathbb{Z}_4 = 2$, implying that $EuBi_4Te_7$ in the A-AFM*x* state is an AXI as well and the quantized bulk orbital magnetoelectric response is expected [77,78]. Furthermore, there is a mirror symmetry operation $\hat{M}_x$ about the $x = 0$ plane in the C_c2/m magnetic space group. Hence, we calculate the mirror Chern numbers (MCNs) via the topological quantum chemistry (TQC) and symmetry indicator (SI) method [79–82]. In our calculations, nontrivial MCNs $C_{\pm i} = \pm 1$ and thus $C_M = 1$ are obtained, suggesting that the A-AFM*x* $EuBi_4Te_7$ is also a magnetic TCI.

It is demonstrated through the bulk-edge correspondence that the nontrivial band topology will give rise to the topological surface/edge states on specific symmetry preserved surface slabs [83]. Hence, we employ the iterative Green function method to calculate the local density of states (LDOS) on the surfaces of $EuBi_4Te_7$. As shown in Fig. 4(a), there are massless Dirac fermion surface states on the (010) surface. These topological surface states, are protected by the $\hat{S}$ and the $\hat{M}_x$ symmetries. On the (001) surface slab, the $\hat{S}$ symmetry is broken but the $\hat{M}_x$ symmetry survives. As a result, massless Dirac cone protected by the mirror symmetry still can be found on the (001) surface, as shown in Fig. 4(b). When turned to the FM*x* configuration, the magnetic space group of $EuBi_4Te_7$ is $C2/m$ (No. 12.58), in which the $\hat{S}$ symmetry is broken down. However, the mirror symmetry $\hat{M}_x$ is preserved. Using the TQC and SI method, we obtain that the MCNs of the $EuBi_4Te_7$ in FM*x* state are $C_{\pm i} = \pm 1$, which are the same as that in A-AFM*x* state. Therefore, protected by the mirror symmetry, the massless Dirac cone surface states still survive on the (010) and (001) surfaces, as shown in Fig. 4(c)(d). The $\hat{S}$ symmetry is preserved in the A-AFM*x* configuration and is broken in the FM configuration. Therefore, the gapless point of the (010) surface states is at the Γ point in A-AFM*x* configuration and slightly deviate from the Γ point in the FM configurations. Furthermore, a nontrivial $\mathbb{Z}_4 = 2$ is obtained no matter in the FM*x* and the FM*z* states throughout our calculations, manifesting the AXI phases in the FM $EuBi_4Te_7$ materials.

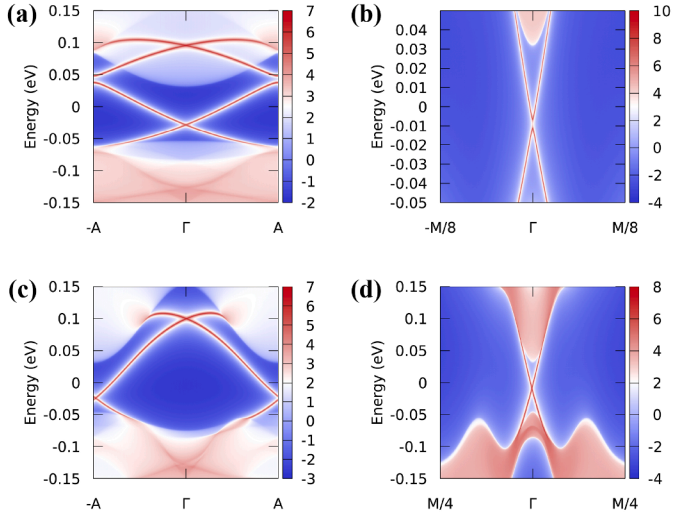

Fig. 6. The simulated surface spectra of $EuSb_4Te_7$. The surface LDOS of $EuSb_4Te_7$ in the A-AFM*z* configuration on **(a)** the (010) surface, **(b)** the (001) surface, in the FM*x* configuration on **(c)** the (010) surface, **(d)** the (001) surface.

Unlike the $EuBi_4Te_7$, the magnetic ground state of the $EuSb_4Te_7$ is the A-AFM*z* configuration, which is of the $P_c\bar{3}c1$ (No. 165.96) magnetic space group. The bulk band structure and the projected band structure of $EuSb_4Te_7$ in the A-AFM*z* configuration are shown in Fig. 5(a)(d). Similar to the $EuBi_4Te_7$, there is an inverted band gap of 87.3 meV between Sb *p* and Te *p* bands near the Γ point, implying the topological nontrivial nature of the $EuSb_4Te_7$ materials. The occupied Eu *f* bands are located at the energy of about 2 eV to 2.5 eV below the Fermi energy, which rarely disentangle with other bands. The bulk band structures of $EuSb_4Te_7$ in the FM*x* and FM*z* configurations are shown in Fig. 5(b)(c), respectively.

In the $P_c\bar{3}c1$ magnetic space group, there are $\hat{P}$ and $\hat{S}$ symmetries as well. In our calculations, nontrivial $\mathbb{Z}_2 = 1$ and $\mathbb{Z}_4 = 2$ are obtained by Eqs. (7) and (8), revealing the AFM TI phase and the AXI phase of $EuSb_4Te_7$. However, since there is no mirror symmetry in the $P_c\bar{3}c1$ magnetic space group, the mirror TCI phase can not exist in the A-AFM*z* $EuSb_4Te_7$ materials. In the FM magnetic configurations, the parity symmetry $\hat{P}$ with AXI phase of $\mathbb{Z}_4 = 2$ survives under the magnetization. In the FM*x* configuration, since the mirror symmetry exists, we can calculate the MCNs via the TQC and SI method. Analogous to the $EuBi_4Te_7$, nontrivial $C_{\pm i} = \pm 1$ MCNs are obtained in our calculations. Thus, the FM*x* $EuSb_4Te_7$ is also a magnetic TCI protected by the mirror symmetry.

Originated from the magnetic symmetry, the $EuSb_4Te_7$ crystals exhibit different surface spectra from that in $EuBi_4Te_7$ in the AFM magnetic ground state. As shown in Fig. 6(a), there are massless Dirac fermion surface dispersions on the $EuSb_4Te_7$ (010) surface, which are

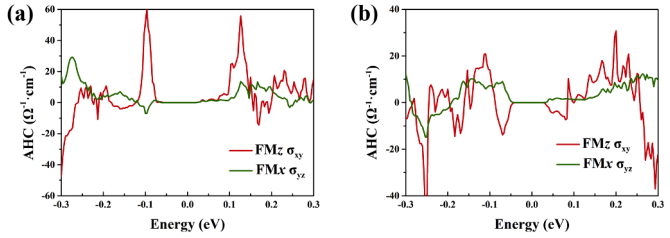

Fig. 7. The anomalous Hall conductivity (AHC). The calculated AHC of **(a)** $EuBi_4Te_7$ and **(b)** $EuSb_4Te_7$.

protected by the $\hat{S}$ symmetry. However, as shown in Fig. 6(b), on the (001) surface, a small band gap is opened as the mirror symmetry is lifted by the z direction magnetization. In the FMx state, as shown in Fig. 6(c)(d), there are massless Dirac cone surface states on the (010) and (001) surfaces similar to that in $EuBi_4Te_7$, as they have the same $C2/m$ magnetic symmetries in this magnetic configuration. Last but not the least, we also calculate the anomalous Hall conductivity (AHC) by the WannierTools package using the following formula:

$$\sigma_{xy} = -\frac{e^2}{\hbar}\int_{BZ}\frac{d^3k}{(2\pi)^3}\Omega^z(\boldsymbol{k}), \tag{9}$$

where $\Omega^z(\boldsymbol{k})$ is the Berry curvature at the $\boldsymbol{k}$ points and the integral runs over all the occupied bands in the whole first Brillouin zone [84]. As shown in Fig. 7(a)(b), significant values of AHC are expected in the FM states of $EuBi_4Te_7$ and $EuSb_4Te_7$ through our calculations, which could be measured experimentally if the materials are electron or hole doped like the experiments on $MnSb_4Te_7$. Since the Chern numbers are zero, the AHC values are zero within the band gap. Notably, there are two peaks of the AHC in $EuBi_4Te_7$ in the FMz state according to our calculations.

Conclusions

In summary, we propose two new-type rare earth magnetic topological vdW material candidates, $EuBi_4Te_7$ and $EuSb_4Te_7$, via first-principles calculations. The simulated phonon dispersions imply that their structures are dynamically stable. In the A-AFM magnetic ground states, coexisting AFM TI phase and AXI phase are unveiled. As a result, massless Dirac fermion dispersions appear on their $\hat{S}$ preserved surfaces. Since the magnetic easy axis of $EuBi_4Te_7$ is along the x direction, a mirror TCI phase with massless Dirac cone surface states are revealed on its (001) vdW terminations as well, facilitating the experimental observations for the topological quasi-particle spectra. When magnetized to the FM states, the AXI phases survive as the parity symmetry $\hat{P}$ preserved. Thus, topological quantized bulk orbital magnetoelectric responses are expected to be obseved in experiments on these condensed matter platforms. Especially, in the FMx configuration, they are all mirror TCIs with massless Dirac cone dispersions on their (010) and (001) surfaces. Notable anomalous Hall conductivities are predicted in their FM states if these materials are electron or hole doped. This work offers more opportunities for the future scientific research and device application of the topological quantum physics and magnetically controllable quantum phase transitions.

CRediT authorship contribution statement

Jia-Yi Lin: Writing – original draft, Validation, Methodology, Investigation, Formal analysis, Data curation, Conceptualization; **Xiao-Bao Yang:** Writing – review & editing; **Yu-Jun Zhao:** Writing – review & editing, Supervision, Software, Resources, Project administration.

Data availability

The data and input files for DFT calculations that support the findings of this study are available upon reasonable request from the authors.

Declaration of competing interest

The authors declare no conflict of financial interest.

Acknowledgement

This work is financially supported by National Natural Science Foundation of China (Grant No. 12474229), and partially supported by High Performance Computing Platform of South China University of Technology.

References

[1] J.E. Moore, The birth of topological insulators, Nature 464 (2010) 194–198.
[2] F.D.M. Haldane, Model for a quantum hall effect without landau levels: condensed-Matter realization of the "parity anomaly, Phys. Rev. Lett. 61 (1988) 2015–2018.
[3] P. Bampoulis, C. Castenmiller, D.J. Klaassen, J.V. Mil, Y. Liu, C.-C. Liu, Y. Yao, M. Ezawa, A.N. Rudenko, H.J.W. Zandvliet, Quantum spin hall states and topological phase transition in germanene, Phys. Rev. Lett. 130 (2023) 196401.
[4] C.-K. Chiu, J.C.Y. Teo, A.P. Schnyder, S. Ryu, Classification of Topological Quantum Matter with Symmetries 88 (2016) 35005.
[5] C.-Z. Chang, J. Zhang, X. Feng, J. Shen, Z. Zhang, M. Guo, K. Li, Y. Ou, P. Wei, L.-L. Wang, et al. Experimental observation of the quantum anomalous hall effect in a magnetic topological insulator, Science 340 (2013) 167–170.
[6] B.Q. Lv, T. Qian, H. Ding, Experimental perspective on three-Dimensional topological semimetals, Rev. Mod. Phys 93 (2021) 25002.
[7] J. Hu, F. Yu, A. Luo, X.-H. Pan, J. Zou, X. Liu, G. Xu, Chiral topological superconductivity in superconductor-Obstructed atomic insulator-Ferromagnetic insulator heterostructures, Phys. Rev. Lett. 132 (2024) 36601.
[8] L. Fu, C.L. Kane, Superconducting proximity effect and majorana fermions at the surface of a topological insulator, Phys. Rev. Lett. 100 (2008) 96407.
[9] M. Sato, Y. Ando, Topological superconductors: a review, Rep. Prog. Phys. 80 (2017) 76501.
[10] H. Zhang, C.-X. Liu, X.-L. Qi, X. Dai, Z. Fang, S.-C. Zhang, Topological insulators in Bi_2PLXSe_3, Bi_2PLXTe_3 and Sb_2PLXTe_3 with a single dirac cone on the surface, Nat. Phys. 5 (2009) 438–442.
[11] T.H. Hsieh, H. Lin, J. Liu, W. Duan, A. Bansil, L. Fu, Topol. Crystalline Insul. SnTe Mater. Class 3 (2012) 1–7.
[12] Z.K. Liu, J. Jiang, B. Zhou, Z.J. Wang, Y. Zhang, H.M. Weng, D. Prabhakaran, S.K. Mo, H. Peng, P. Dudin, et al. A Stab. Three-Dimens. Topol. Dirac Semimetal Cd_3PLXAs_2 13 (2014) 677–681.
[13] Z.K. Liu, B. Zhou, Y. Zhang, Z.J. Wang, H.M. Weng, D. Prabhakaran, S.-K. Mo, Z.X. Shen, Z. Fang, X. Dai, et al. Discovery of a three-dimensional topological dirac semimetal, Na_3PLXBi 343 (2014) 864–867.
[14] H. Weng, C. Fang, Z. Fang, B.A. Bernevig, X. Dai, Weyl semimetal phase in noncentrosymmetric transition-metal monophosphides, 2015, p. 11029. 5.
[15] B.Q. Lv, N. Xu, H.M. Weng, J.Z. Ma, P. Richard, X.C. Huang, L.X. Zhao, G.F. Chen, C.E. Matt, F. Bisti, et al. Observation of weyl nodes in taas, Nat. Phys. 11 (2015) 724–727.
[16] F. Schindler, A.M. Cook, M.G. Vergniory, Z. Wang, S.S.P. Parkin, B.A. Bernevig, T. Neupert, 4, 2018.
[17] F. Schindler, Z. Wang, M.G. Vergniory, A.M. Cook, A. Murani, S. Sengupta, A.Y. Kasumov, R. Deblock, S. Jeon, I. Drozdov, et al. Higher-order topology in bismuth, Nat. Phys. 14 (2018) 918–924.
[18] C. Chen, X.-T. Zeng, Z. Chen, Y.X. Zhao, X.-L. Sheng, S.A. Yang, Second-order real nodal-Line semimetal in three-dimensional graphdiyne, Phys. Rev. Lett. 128 (2022) 26405.
[19] P.C. Sreeparvathy, R.A.B. Villaos, Z.-Q. Huang, F.-C. Chuang, Higher-order Topol. Dirac Phase in $Y_3PLXInC$: a First-princ. Study 26 (2024) 73007.
[20] S. Nie, J. Chen, C. Yue, C. Le, D. Yuan, Z. Wang, W. Zhang, H. Weng, Tunable Dirac Semim. Higher-order Fermi Arcs in Kagome Lattices $Pd_3PLXPb_2PLXX_2$ X = S (2022) 1958–1961.
[21] T. Zhang, Y. Jiang, Z. Song, H. Huang, Y. He, Z. Fang, H. Weng, C. Fang, Catalogue of Topological Electronic Materials 566 (2019) 475–479. Nature.
[22] F. Tang, H.C. Po, A. Vishwanath, X. Wan, Comprehensive search for topological materials using symmetry indicators, Nature 566 (2019) 486–489.
[23] M.G. Vergniory, L. Elcoro, C. Felser, N. Regnault, B.A. Bernevig, Z. Wang, A complete catalogue of high-quality topological materials, Nature 566 (2019) 480–485.
[24] M.G. Vergniory, B.J. Wieder, L. Elcoro, S.S.P. Parkin, C. Felser, B.A. Bernevig, N. Regnault, All topological bands of all nonmagnetic stoichiometric materials, Science 376 (2022) 9094.
[25] Y. Xu, M.G. Vergniory, D.-S. Ma, J.L.M. nes, Z.-D. Song, B.A. Bernevig, N. Regnault, L. Elcoro, Catalog of Topol. Phonon Mater. 384 (2024) 8458. Science.
[26] D.R. Hofstadter, Energy levels and wave functions of bloch electrons in rational and irrational magnetic fields, Phys. Rev. B 14 (1976) 2239.

[27] Y.-Y. Zhang, X.-R. Wang, X.C. Xie, Three-dimensional topological insulator in a magnetic field: chiral side surface states and quantized hall conductance, J. Phys. Condens. Matter 24 (2011) 15004.

[28] R.S.K. Mong, A.M. Essin, J.E. Moore, Antiferromagnetic topological insulators, Phys. Rev. B 81 (2010) 245209.

[29] M.M. Otrokov, I.I. Klimovskikh, H. Bentmann, D. Estyunin, A. Zeugner, Z.S. Aliev, S. Gaß, A.U.B. Wolter, A.V. Koroleva, A.M. Shikin, et al. Prediction and observation of an antiferromagnetic topological insulator, Nature 576 (2019) 416–422.

[30] D. Zhang, M. Shi, T. Zhu, D. Xing, H. Zhang, J. Wang, Topological axion states in the magnetic insulator $MnBi_2PLXTe_4$ with the quantized magnetoelectric effect, Phys. Rev. Lett. 122 (2019) 206401.

[31] S. Yang, X. Xu, Y. Zhu, R. Niu, C. Xu, Y. Peng, X. Cheng, X. Jia, Y. Huang, X. Xu, J. Lu, Y. Ye, Odd-even layer-Number effect and layer-dependent magnetic phase diagrams in $MnBi_2PLXTe_4$, Phys. Rev. X 11 (2021) 11003.

[32] Y. Deng, Y. Yu, M.Z. Shi, Z. Guo, Z. Xu, J. Wang, X.H. Chen, Y. Zhang, Quantum Anomalous Hall Effect in Intrinsic Magnetic Topological Insulator $MnBi_2PLXTe_4$ 367 (2020) 895–900.

[33] Z. Zang, Y. Zhu, M. Xi, S. Tian, T. Wang, P. Gu, Y. Peng, S. Yang, X. Xu, Y. Li, B. Han, L. Liu, Y. Wang, P. Gao, J. Yang, H. Lei, Y. Huang, Y. Ye, Layer-Number-Dependent antiferromagnetic and ferromagnetic behavior in $MnSb_2PLXTe_4$, Phys. Rev. Lett. 128 (2022) 17201.

[34] T. Zhu, A.J. Bishop, T. Zhou, M. Zhu, D.J. O'hara, A.A. Baker, S. Cheng, R.C. Walko, J.J. Repicky, T. Liu, et al. Synthesis, Magnetic Prop. Electronic Struct. Mag. Topol. Insulator $MnBi_2PLXSe_4$ 21 (2021) 5083–5090.

[35] F. Zhan, Z. Qin, D.-H. Xu, X. Zhou, D.-S. Ma, R. Wang, Design of antiferromagnetic second-Order band topology with rotation topological invariants in two dimensions, Nano Lett. 24 (2024) 7741–7747.

[36] R.C. Vidal, H. Bentmann, J.I. Facio, T. Heider, P. Kagerer, C.I. Fornari, T.R.F. Peixoto, T. Figgemeier, S. Jung, C. Cacho, B. Büchner, J.V.D. Brink, C.M. Schneider, L. Plucinski, E.F. Schwier, K. Shimada, M. Richter, A. Isaeva, F. Reinert, Orbital complexity in intrinsic magnetic topological insulators $MnBi_4PLXTe_7$ and $MnBi_6PLXTe_{10}$, Phys. Rev. Lett. 126 (2021) 176403.

[37] C. Hu, L. Ding, K.N. Gordon, B. Ghosh, H.-J. Tien, H. Li, A.G. Linn, S.-W. Lien, C.-Y. Huang, S. Mackey, et al. Realization of an Intrinsic Ferromagnetic Topological State in $MnBi_8PLXTe_{13}$ 6 (2020) 4275.

[38] S.V. Eremeev, I.P. Rusinov, Y.M. Koroteev, A.Y. Vyazovskaya, M. Hoffmann, P.M. Echenique, A. Ernst, M.M. Otrokov, E.V. Chulkov, Topological magnetic materials of the $(MnSSb_2PLXTe_4)(Sb_2PLXTe_3)_n$ van der Waals compounds family, J. Phys. Chem. Lett. 12 (2021) 4268–4277.

[39] C. Hu, K.N. Gordon, P. Liu, J. Liu, X. Zhou, P. Hao, D. Narayan, E. Emmanouilidou, H. Sun, Y. Liu, et al. A van der Waals antiferromagnetic topological insulator with weak interlayer magnetic coupling, Nat. Commun. 11 (2020) 1–8.

[40] S. Huan, S. Zhang, Z. Jiang, H. Su, H. Wang, X. Zhang, Y. Yang, Z. Liu, X. Wang, N. Yu, et al. Multiple magnetic topological phases in bulk van der waals crystal $MnSb_4PLXTe_7$, Phys. Rev. Lett. 126 (2021) 246601.

[41] M. Rodriguez-Vega, Z.-X. Lin, A. Leonardo, A. Ernst, M.G. Vergniory, G.A. Fiete, Light-Driven topological and magnetic phase transitions in thin layer antiferromagnets, J. Phys. Chem. Lett. 13 (2022) 4152–4158.

[42] J.-Y. Lin, Z.-J. Chen, W.-Q. Xie, X.-B. Yang, Y.-J. Zhao, Toward ferromagnetic semimetal ground state with multiple weyl nodes in van der waals crystal $MnSb_4PLXTe_7$, New J. Phys. 24 (2022) 43033.

[43] Y. Li, Y. Jiang, J. Zhang, Z. Liu, Z. Yang, J. Wang, Intrinsic topological phases in $Mn_2PLXBi_2PLXTe_5$ tuned by the layer magnetization, Phys. Rev. B 102 (2020) 121107.

[44] L. Cao, S. Han, Y.-Y. Lv, D. Wang, Y.-C. Luo, Y.-Y. Zhang, S.-H. Yao, J. Zhou, Y.B. Chen, H. Zhang, Y.-F. Chen, Growth and characterization of the dynamical axion insulator candidate $Mn_2PLXBi_2PLXTe_5$ with intrinsic antiferromagnetism, Phys. Rev. B 104 (2021) 54421.

[45] S.V. Eremeev, M.M. Otrokov, A. Ernst, E.V. Chulkov, Magnetic Ordering and Topology in $Mn_2PLXBi_2PLXTe_5$ and $Mn_2PLXSb_2PLXTe_5$ van der Waals Materials 105 (2022) 195105.

[46] J. Zhang, D. Wang, M. Shi, T. Zhu, H. Zhang, J. Wang, Large dynamical axion field in topological antiferromagnetic insulator $Mn_2PLXBi_2PLXTe_5$, Chin. Phys. Lett. 37 (2020) 77304.

[47] J. Li, C. Wang, Z. Zhang, B.-L. Gu, W. Duan, Y. Xu, Magnetically controllable topological quantum phase transitions in the antiferromagnetic topological insulator $MnBi_2PLXTe_4$, Phys. Rev. B 100 (2019) 121103.

[48] J.-Y. Lin, Z.-J. Chen, Z. Cao, J. Zeng, X.-B. Yang, Y. Yao, Y.-J. Zhao, Multiple magnetic topological phases in the van der waals crystal $Mn(Bi,Sb)_4PLXSe_7$, J. Phys. Chem. Lett. 14 (2023) 3913–3919.

[49] J.-Y. Lin, Z. Cao, Z.-J. Chen, W. He, J. Zeng, X.-B. Yang, Y. Hua, J.-H. Liao, Y.-J. Zhao, Topological crystalline insulator phases in magnetic van der waals crystal $MnBi_4PLXte_7$ and $mn_2PLXBi_2PLXTe_5$ families, J. Phys. Chem. C 128 (2024) 20451–20458.

[50] H. Deng, Z. Chen, A.W. oś, M. Konczykowski, K. Sobczak, J. Sitnicka, I.V. Fedorchenko, J. Borysiuk, T. Heider, L. Pluciński, et al. High-Temperature quantum anomalous hall regime in a $MnBi_2PLXTe_4/Bi_2PLXTe_3$ superlattice, Nat. Phys. 17 (2021) 36–42.

[51] G. Kresse, J. Furthmüller, Efficiency of ab-initio total energy calculations for metals and semiconductors using a plane-Wave basis set, Comput. Mater. Sci. 6 (1996) 15–50.

[52] G. Kresse, J. Hafner, Ab initio molecular dynamics for open-Shell transition metals, Phys. Rev. B 48 (1993) 13115–13118.

[53] G. Kresse, J. Hafner, Ab initio molecular dynamics for liquid metals, Phys. Rev. B 47 (1993) 558–561.

[54] J.P. Perdew, K. Burke, M. Ernzerhof, Generalized gradient approximation made simple, Phys. Rev. Lett. 77 (1996) 3865–3868.

[55] G. Kresse, D. Joubert, From ultrasoft pseudopotentials to the projector augmented-Wave method, Phys. Rev. B 59 (1999) 1758–1775.

[56] P.E. Blöchl, Projector augmented-Wave method, Phys. Rev. B 50 (1994) 17953–17979.

[57] G. Kresse, J. Furthmüller, Efficient iterative schemes for ab initio total-Energy calculations using a plane-Wave basis set, Phys. Rev. B 54 (1996) 11169–11186.

[58] V.I. Anisimov, J. Zaanen, O.K. Andersen, B. Theory, M. Insulators, 44, Hubbard U Instead of Stoner I, 1991.

[59] S.L. Dudarev, G.A. Botton, S.Y. Savrasov, C.J. Humphreys, A.P. Sutton, Electron-Energy-Loss spectra and the structural stability of nickel oxide: an LSDA u study, Phys. Rev. B 57 (1998) 1505–1509.

[60] J.W. Furness, A.D. Kaplan, J. Ning, J.P. Perdew, J. Sun, Accurate and numerically efficient r^2PLXSCAN meta-Generalized gradient approximation, J. Phys. Chem. Lett. 11 (2020) 8208–8215.

[61] S. Ehlert, U. Huniar, J. Ning, J.W. Furness, J. Sun, A.D. Kaplan, J.P. Perdew, J.G. Brandenburg, Dispersion corrected meta-generalized gradient approximation for general chemical applications, ^{2}PLXscan 4 (2021) 61101.

[62] E. Caldeweyher, J.-M. Mewes, S. Ehlert, S. Grimme, Extension and evaluation of the D4 london-Dispersion model for periodic systems, Phys. Chem. Chem. Phys. 22 (2020) 8499–8512.

[63] E. Caldeweyher, S. Ehlert, A. Hansen, H. Neugebauer, S. Spicher, C. Bannwarth, S. Grimme, A generally applicable atomic-Charge dependent london dispersion correction, J. Chem. Phys. 150 (2019) 154122.

[64] J. Gao, Q. Wu, C. Persson, Z. Wang, Irvsp: to obtain irreducible representations of electronic states in the VASP, Comput. Phys. Comm. 261 (2021) 107760.

[65] J. Gao, Z. Guo, H. Weng, Z. Wang, Magnetic band representations, fu-Kane-Like symmetry indicators, and magnetic topological materials, Phys. Rev. B 106 (2022) 35150.

[66] G. Pizzi, V. Vitale, R. Arita, S. Blügel, F. Freimuth, G. Géranton, M. Gibertini, D. Gresch, C. Johnson, T. Koretsune, et al. Wannier90 as a Community Code: New Features and Applications 32 (2020) 165902.

[67] N. Marzari, D. Vanderbilt, Maximally localized generalized wannier functions for composite energy bands, Phys. Rev. B 56 (1997) 12847–12865.

[68] I. Souza, N. Marzari, D. Vanderbilt, Maximally localized wannier functions for entangled energy bands, Phys. Rev. B 65 (2001) 35109.

[69] Q. Wu, S. Zhang, H.-F. Song, M. Troyer, A.A. Soluyanov, Wanniertools: an open-Source software package for novel topological materials, Comput. Phys. Comm 224 (2018) 405–416.

[70] M.P.L. Sancho, J.M.L. Sancho, J.M.L. Sancho, J. Rubio, Highly convergent schemes for the calculation of bulk and surface green functions, J. Phys. F Met. Phys. 15 (1985) 851.

[71] J. Li, Y. Li, S. Du, Z. Wang, B.-L. Gu, S.-C. Zhang, K. He, W. Duan, Y. Xu, Intrinsic magnetic topological insulators in van der Waals layered $MnBi_2PLXTe_4$-family materials 5 (2019) 5685.

[72] O. Kabi, M.S. Abu-Jafar, M. Farout, A.A. Mousa, A. Bouhemadou, N. Erum, S.M. Azar, A. Bassalat, H. Abualrob, A.Y. Thabaineh, et al. Ab initio investigation of the structural, elastic, dynamic, electronic, and magnetic properties of cubic perovskite $cecro_3$, ACS Omega 9 (2024) 11820–11828.

[73] D.V. Suetin, I.R. Shein, Electronic structure, mechanical and dynamical stability of hexagonal subcarbides m_2PLXc (M= Tc, Ru, Rh, Pd, Re, Os, Ir, and Pt): ab initio calculations, Phys. Solid State 60 (2018) 213–224.

[74] C. Fang, M.J. Gilbert, B.A. Bernevig, Topological insulators with commensurate antiferromagnetism, Phys. Rev. B 88 (2013) 85406.

[75] C. Yue, Y. Xu, Z. Song, H. Weng, Y.-M. Lu, C. Fang, X. Dai, Symmetry-Enforced chiral hinge states and surface quantum anomalous hall effect in the magnetic axion insulator $Bi_{2-x}PLXSm_xPLXSe_3$, Nat. Phys. 15 (2019) 577–581.

[76] Y. Xu, Z. Song, Z. Wang, H. Weng, X. Dai, Higher-Order topology of the axion insulator $euin_2PLXAs_2$, Phys. Rev. Lett 122 (2019) 256402.

[77] A.M. Essin, J.E. Moore, D. Vanderbilt, Magnetoelectric polarizability and axion electrodynamics in crystalline insulators, Phys. Rev. Lett. 102 (2009) 146805.

[78] A. Malashevich, I. Souza, S. Coh, D. Vanderbilt, Theory of orbital magnetoelectric response, New J. Phys 12 (2010) 53032.

[79] B. Peng, Y. Jiang, Z. Fang, H. Weng, C. Fang, Topological classification and diagnosis in magnetically ordered electronic materials, Phys. Rev. B 105 (2022) 235138.

[80] B. Bradlyn, L. Elcoro, J. Cano, M.G. Vergniory, Z. Wang, C. Felser, M.I. Aroyo, B.A. Bernevig, Topol. Quant. Chem. 547 (2017) 298–305.

[81] Y. Xu, L. Elcoro, Z.-D. Song, B.J. Wieder, M.G. Vergniory, N. Regnault, Y. Chen, C. Felser, B.A. Bernevig, High-Throughput calculations of magnetic topological materials, Nature 586 (2020) 702–707.

[82] L. Elcoro, B.J. Wieder, Z. Song, Y. Xu, B. Bradlyn, B.A. Bernevig, Magnetic topological quantum chemistry, Nat. Commun. 12 (2021) 1–10.

[83] L. Fu, C.L. Kane, Time reversal polarization and a Z_2 adiabatic spin pump, Phys. Rev. B 74 (2006) 195312.

[84] Y. Yao, L. Kleinman, A.H. Macdonald, J. Sinova, T. Jungwirth, D.-S. Wang, E. Wang, Q. Niu, First principles calculation of anomalous hall conductivity in ferromagnetic bcc fe, Phys. Rev. Lett. 92 (2004) 37204.